


GO/TiO₂ composites as a highly active photocatalyst for the degradation of methyl orange

Chunling Lin^{1,a)}, Yifeng Gao², Jiaoxia Zhang^{2,b)} , Dan Xue¹, Hua Fang¹, Jiayong Tian¹, Chunli Zhou¹, Chanjuan Zhang¹, Yuqing Li^{3,c)}, Honggang Li⁴

¹School of Chemistry and Chemical Engineering, Xi'an Shiyou University, Xi'an 710065, China

²School of Materials Science and Engineering, Jiangsu University of Science and Technology, Zhenjiang 212003, China

³Testing Center, Yangzhou University, Yangzhou 225009, China

⁴China Railway Design Corporation, Tianjin 300251, China

^{a)}Address all correspondence to these authors. e-mail: chunling405@xsyu.edu.cn

^{b)}e-mail: zhangjx@just.edu.cn

^{c)}e-mail: liyuqing@yzu.edu.cn

Received: 29 January 2020; accepted: 31 January 2020

Reduced graphene oxide supported titanium dioxide (GO/TiO₂) heterojunction composites as highly active photocatalysts were synthesized via simple ultrasonic mixing and hydrothermal reaction using TiCl₃ and GO as precursors. Their structure and morphology were characterized by X-ray diffraction, Fourier transform infrared spectroscopy, Raman spectra, UV-vis spectroscopy, and thermogravimetric analysis. The GO/TiO₂ heterojunction composites were used to degrade methyl orange (MO). The adsorption and photocatalytic degradation rate of the prepared GO/TiO₂ composites increased by nearly three times compared with that of pristine TiO₂ or GO, which reached up 90%, to degrade MO after 4 h, which provides a simple method to obtain photocatalytic materials.

Introduction

Photocatalytic technology is one of the most effective methods for wastewater treatment because of its low investment cost, mild reaction conditions, and negligible secondary pollution to the environment [1, 2, 3, 4, 5, 6]. Preparation of photocatalysts with high photocatalytic activity and photochemical stability is the key factor to boost practical applications of semiconductor photocatalysts [7, 8, 9, 10, 11, 12]. Among well-known photocatalysts, titanium dioxide (TiO₂) exhibits excellent photocatalytic properties, long-term stability, non-toxicity, chemical inertness, and low cost [13]. Therefore, TiO₂ has been widely used in photocatalytic studies [14, 15, 16, 17, 18, 19, 20]. However, some serious shortcomings still need to be overcome. For example, TiO₂ has a large band gap (the rutile and anatase phases are 3.03 and 3.20 eV, respectively), which can absorb only ultraviolet light (approximately 5% of solar light) [21]. Meanwhile, its photogenerated electron-hole pairs are easy to recombine. Many researchers have focused on the modification of TiO₂ to obtain new types of highly active photocatalysts that can work under visible light [22, 23, 24, 25, 26, 27]. Many attempts have been

performed to enhance the visible light photocatalytic efficiency of TiO₂, including metal or nonmetal doping [28, 29, 30, 31], dye sensitization [32], surface modification [33, 34], and coupling with other semiconductor materials [35, 36, 37]. Among these methods, the coupling of TiO₂ with guest semiconductors is an effective way to improve its photocatalytic activity under visible light [21].

Graphene is a two-dimensional allotrope of crystalline carbon formed by hexagonally arranging sp²-bonded carbon atoms, which presents excellent optical properties, transparency, mechanical flexibility, and good thermal and chemical stability [38]. Graphene oxide (GO), an oxidized derivative of graphene, is a promising carbon material that has attracted significant interest over the last decade. When graphene is heavily oxygenated to generate GO, a number of functional groups on its basal planes, such as hydroxyl and epoxies, in addition to carbonyl and carboxyl groups located at the sheet edges, are formed [39]. The presence of these functional groups makes GO sheets strongly hydrophilic, allowing GO to readily exfoliate in water or solvents to produce stable dispersions [40, 41]. GO sheets possessing oxygenated functional groups anchor

active materials easily, and large surface areas focus some potential supported materials on nanomaterials to prevent their aggregation [42, 43, 44, 45, 46, 47, 48, 49, 50, 51, 52]. TiO₂-RGO nanocomposites were fabricated using either isopropyl (IsoprOH) or ethyl (EtOH) alcohol. The photocatalytic properties of the prepared materials using IsoprOH had smaller crystallite size, narrower apparent band gap, smaller isoelectric point, larger adsorption capacity, and higher photocatalytic activity [53]. In Ag₃VO₄/C₃N₄/reduced TiO₂ microsphere ternary composites, the introduction of Ag₃VO₄ into g-C₃N₄/r-TiO₂ can effectively improve the photocatalytic activity of degradation of methylene blue, compared with single component and C₃N₄/reduced TiO₂ binary composites, due to a synergistic effect including the formation of a heterojunction, large surface area, improved light absorption, matched energy band structure, and improved separation efficiency of photogenerated charges coming from the dual Z-scheme structure [54].

In this study, GO/TiO₂ composites were synthesized using TiCl₃ and graphite as raw materials via hydrothermal reaction.

The phase composition, morphology, and thermal stability of the prepared GO/TiO₂ were investigated by X-ray diffraction (XRD), Fourier transform infrared spectroscopy (FTIR), and thermogravimetric analysis (TGA). In addition, their photocatalytic activities were evaluated via ultraviolet-visible (UV-vis) spectroscopy based on degraded methyl orange (MO) dye. The GO/TiO₂ composites evidently degraded 90% of MO.

Results and discussion

The characterization of GO/TiO₂ composites

Fig. 1(a) shows the FTIR spectra of GO and GO/TiO₂ composites. In the GO spectrum, a broad band appears at around 3423 cm⁻¹, which is due to the O-H stretching vibration, and a peak at 1730 cm⁻¹, which could be assigned to the carbonyl C=O stretching vibration. The peaks at 1620 cm⁻¹ and 1226 cm⁻¹ are attributed to C=C vibrations and C-O-C stretching vibrations, respectively. The peak at 1049 cm⁻¹ for the C-O stretching vibration appears due to the presence of epoxide groups on the GO layer. However, the

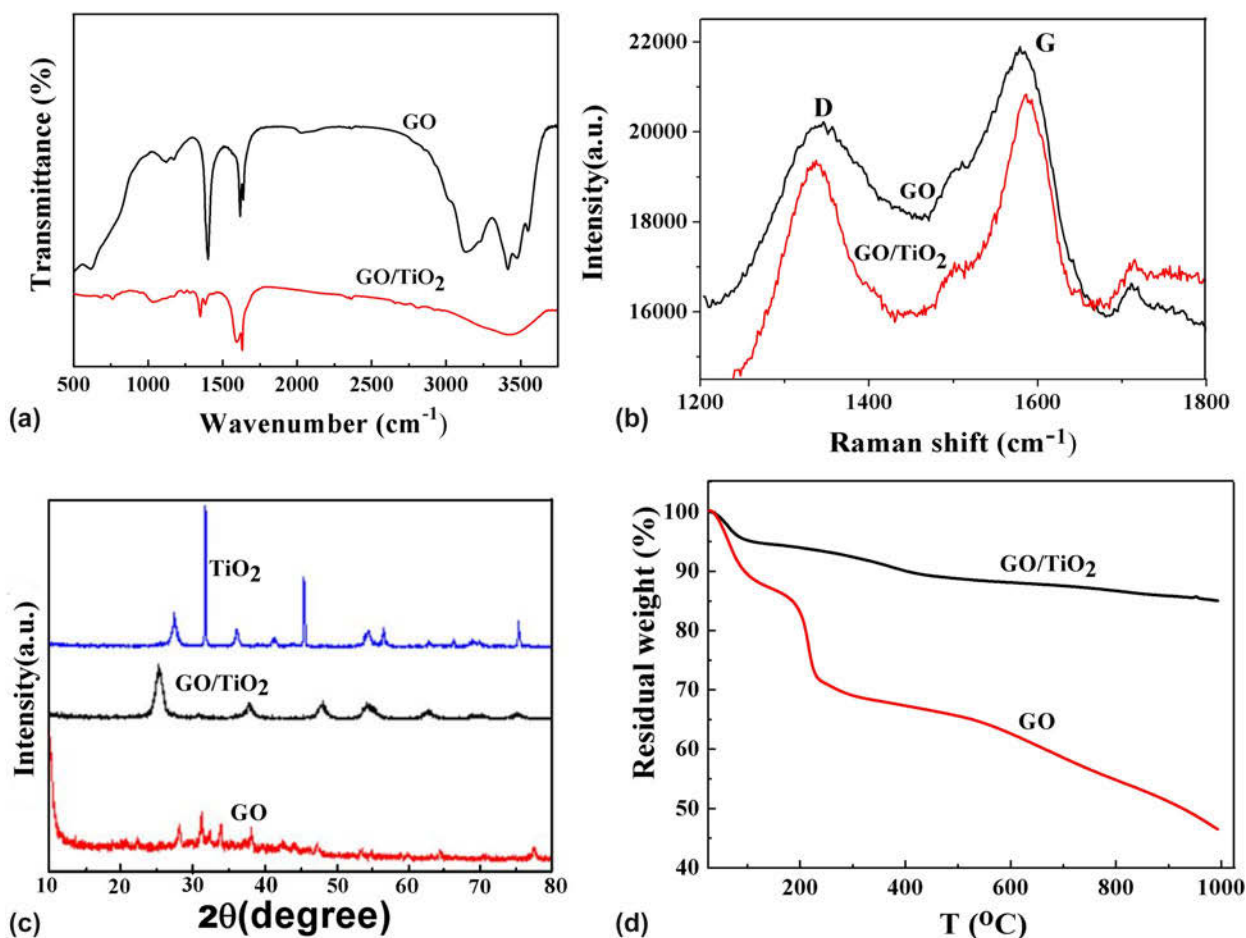


Figure 1: (a) FTIR spectra, (b) Raman spectra, (c) XRD patterns, (d) TGA of GO and GO/TiO₂ composites.

strength of the vibration peaks of the main oxygen functional groups of GO in GO/TiO₂ composites is obviously weakened, which indicates that GO has a certain degree of reduction during the hydrothermal process.

For the Raman spectra of GO and GO/TiO₂ composites [Fig. 1(b)], it can be seen that the GO and GO/TiO₂ have D and G peaks at 1348 and 1586 cm⁻¹, respectively. The peak intensities of I_D/I_G for GO and GO/TiO₂ are 0.925 and 0.921, respectively. So, the GO/TiO₂ exhibits a higher regularity than GO due to the reduction of GO during the hydrothermal process to decrease the oxygen content on the surface of GO. It further indicates that the number of sp² hybrid carbon atoms in GO is more than that of sp³ hybrid carbon atoms in the GO/TiO₂ composites [55].

The TGA curves of GO and GO/TiO₂ composites are shown in Fig. 1(d) to evaluate their thermal stability. For the two samples, the TGA curves have three weight loss stages. For the GO, the first weight loss at about 25–120 °C is caused by the volatilization of absorbed water in materials. The content of combined water is about 12 wt% due to hydrophilic groups. The second weight loss at about 120–210 °C is sharp and caused by the decomposition of the oxygen groups present such as C=O, C–O, and epoxy groups, which reaches up to 14 wt%. The second weight loss at about 220–1000 °C is due to the decomposition of the carbon and carbon skeleton in GO. Their decomposition is serious due to the carbonization of a great amount of sp² and sp³ hybrid carbon atoms even after 1000 °C. In contrast, the GO/TiO₂ composites

exhibit obvious thermal stability. The content of absorbed water is about 5 wt%. The oxygen groups present only cause about 5 wt% of decomposition. Decomposition of the carbon and carbon skeleton is faint, and the GO/TiO₂ composites remain about 90 wt% after 1000 °C. These indicate that the thermal stability of GO/TiO₂ composites is higher than that of GO. The decrease in the oxygen groups present results from the loading TiO₂ consuming oxygen groups and reduction of some containing oxygen groups after the hydrothermal treatment.

Fig. 1(c) shows the XRD spectra of GO and GO/TiO₂ composites. There is a strong peak near 2θ = 32°, which is the diffraction peak of graphite surface (002). The sharp peak near 2θ = 12° indicates that the structure of GO (001) contains a lot of defects and containing oxygen groups. The oxygen groups are beneficial to further load TiO₂ nanoparticles. For the GO/TiO₂ composites, the sharp peak near 2θ = 125° comes from the (002) face of anatase TiO₂. So, the prepared sample is anatase TiO₂ with high photocatalytic ability. In addition, the diffraction peaks corresponding to the crystal faces of TiO₂ (003), (004), (005), (006), (007), and (008) are also found in the vicinity of 35–40°, 49–55°, 62–65°, 68–70°, and 75°, respectively. Therefore, TiO₂ was formed on the surface of GO by redox reaction with TiCl₃ in solution. However, the peaks of GO cannot be found because the intensity of TiO₂ is obviously higher than that of GO [56, 57, 58, 59, 60, 61, 62].

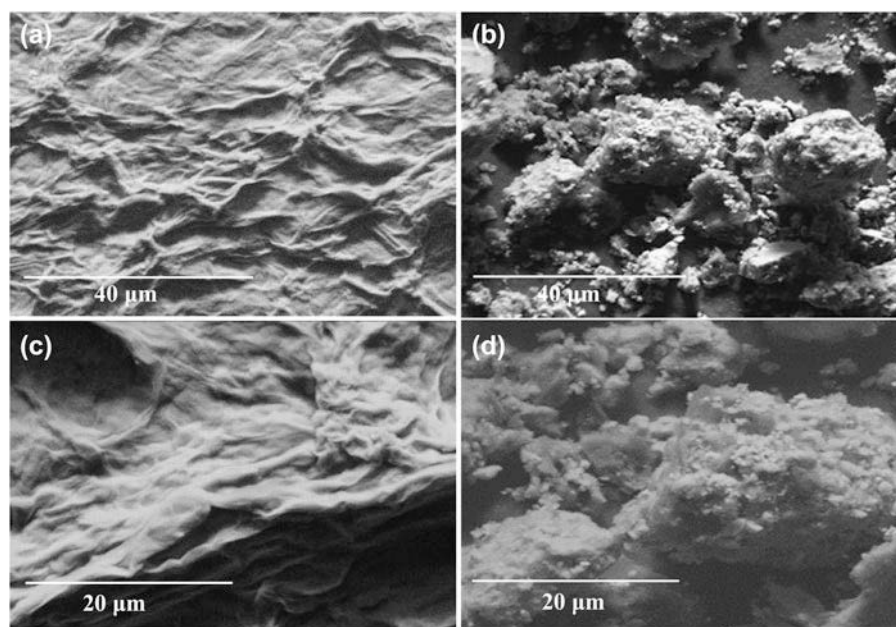


Figure 2: SEM images of GO (a, c) and GO/TiO₂ composites (b, d).

Fig. 2 is the scanning electron microscope (SEM) images of GO and GO/TiO₂. It can be seen from Figs. 2(a) and 2(c) that the GO sheet has the obvious folds. A large number of spherical particles are formed on the surface of partially reduced GO [Figs 2(b) and 2(d)]. Combining with GO [Figs 2(a) and 2(c)], it can be concluded that the addition of graphene effectively inhibits the agglomeration of TiO₂ particles, promoting uniform dispersion of TiO₂ on the surface of GO sheets.

The adsorption–desorption isotherm and the corresponding BET pore diameter distribution curves of the sample are shown in Fig. 3. It can be seen from Fig. 3(a) that the adsorption increases with the increase in pressure. As shown in Fig. 3(b), all the isothermal adsorption–desorption curves show type-IV isotherms shape at a relative pressure range of 0.42–0.95. This clearly indicates that the samples are mesoporous materials with multilayer adsorption.

Photocatalytic activity of GO/TiO₂ composites

UV-vis spectroscopy is implemented to estimate the optical absorption ability of GO/TiO₂ nanocomposites. The UV-vis spectra of GO and GO/TiO₂ are given as Fig. 4(a). For the GO, the absorption peak is at 235 nm. For the GO/TiO₂ composites, the maximum absorptivity is at 240 nm, which is a red shift, and their intensity is higher than that of GO. It indicates the increased photocatalytic efficiency when the TiO₂ load onto the surface of GO. In addition, they also have another absorption peak at 302 nm due to the photocatalytic activity of TiO₂. Therefore, the composites are expected to improve the photocatalytic activity, which will be verified in the photocatalytic degradation of methylene orange dye.

The degradation ratio of GO/TiO₂ for MO is studied, as shown in Fig. 4(b). First, the MO degradation efficiency of

GO/TiO₂ composites in sunlight and under a 48W ultraviolet light was determined. The degradation ratio of MO from ultraviolet irradiation is 85.73%, while that in sunlight is 40% [Fig. 4(b)], which is obviously lower than that in ultraviolet light because it is difficult to excite electron-hole pairs at a low energy in sunlight. Fig. 4(c) shows the MO degradation ratio of three samples in ultraviolet irradiation for 4 h. However, the GO and TiO₂ display similar degradation ratios (36.8% and 38.5%, respectively), and GO/TiO₂ composites display 85.4% degradation ratios after 4 h. For GO, the degradation ratio mainly depends on the adsorption of GO, and the degradation ratio remains unchanged when the adsorption reaches equilibrium. TiO₂ nanomaterials eliminate the MO in solution via degradation reaction of active groups under ultraviolet light. Therefore, the GO and TiO₂ display lower degradation ratios than GO/TiO₂ composites. The degradation ratio of GO/TiO₂ is the fastest within 1 h, resulting from the adsorption of GO via π - π interaction between GO and MO. The MO transfer from solution to the surface of GO/TiO₂ occurs in the first 1 h. The adsorption reaction reached equilibrium after 1 h, so the degradation ratio increased linearly with time. In addition, GO/TiO₂ has a micro-mesoporous structure, which further increases its specific surface area, and also has physical adsorption on MO, and it is multilayer adsorption. Finally, in the solution, the active group produced by embedding TiO₂ on GO surface can be rapidly combined with MO, which can also promote the degradation of MO.

In order to further increase the degradation ratio of MO, 2 mL hydrogen peroxide (H₂O₂) was added into the solution to evaluate the influence of hydrogen peroxide on the photodegradation rate, which is shown in Fig. 4(d). The MO degradation ratio of GO/TiO₂ increased with the irradiation time. Approximately 40% of MO was degraded by GO/TiO₂ composites in the absence of H₂O₂ after 4 h. In comparison,

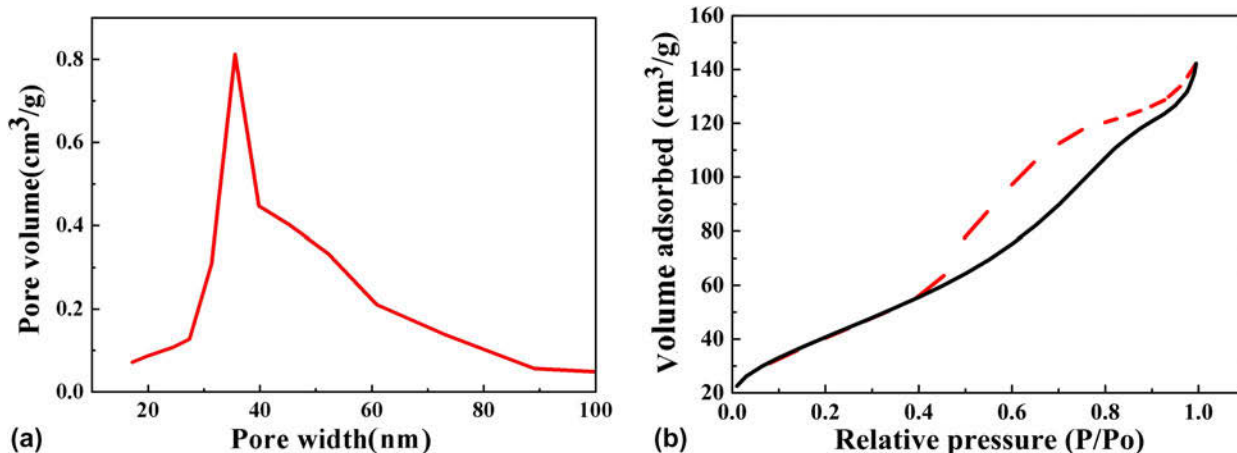


Figure 3: (a) Distribution of pore size and (b) adsorption–desorption curve of GO/TiO₂ composites.

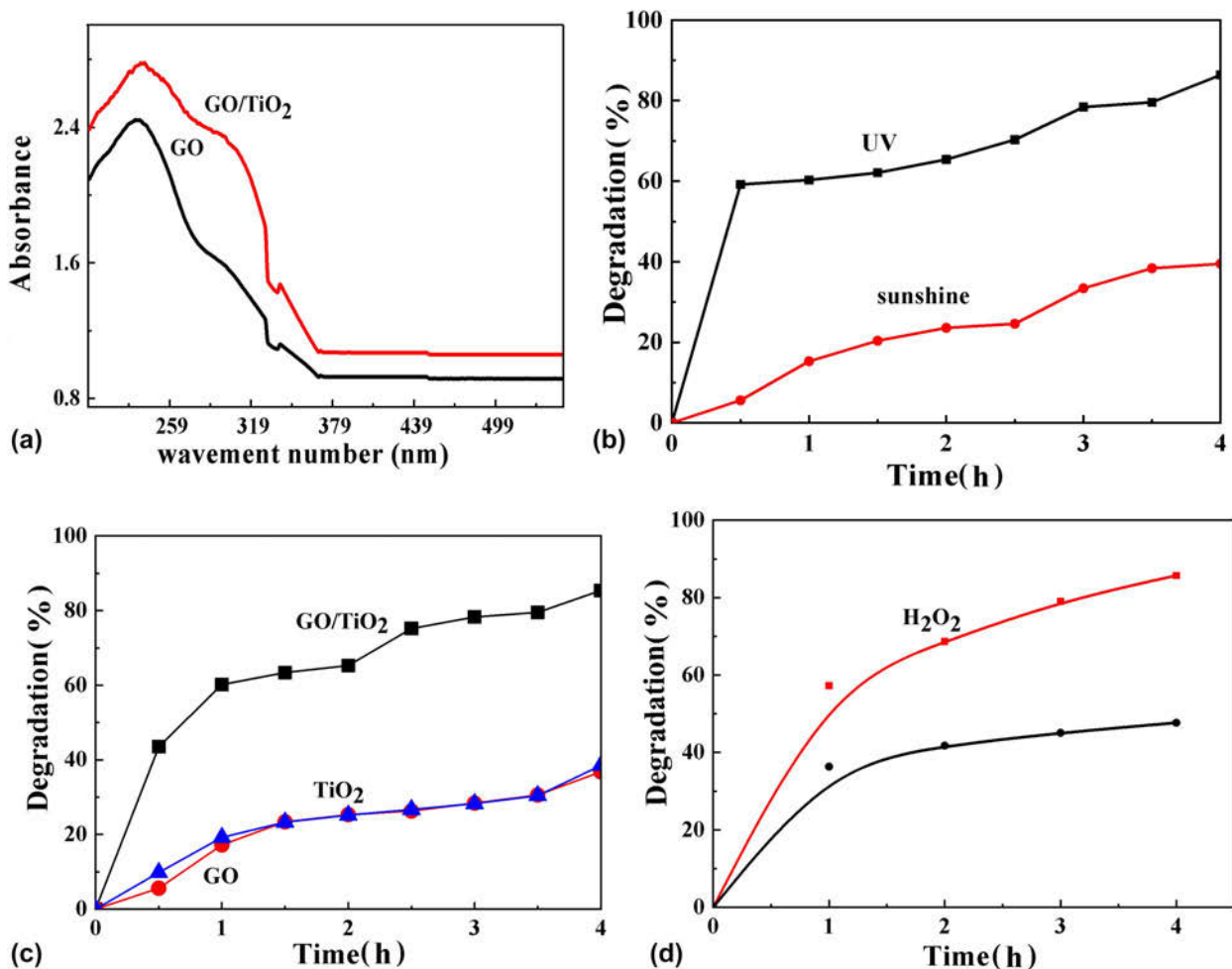


Figure 4: UV-vis spectra of GO and GO/TiO₂ composites (a), photocatalytic degradation of MO in sunlight and 48-W UV light irradiation by GO/TiO₂ composites (b), photocatalytic degradation of GO, TiO₂, and GO/TiO₂ composites in 48-W UV light irradiation (c), influence of H₂O₂ on the degradation of MO with GO/TiO₂ composites in sunlight (d).

90% of MO was degraded when hydrogen peroxide was dripped into the solution. Hydrogen peroxide promotes the rapid formation of OH radical groups to degrade more MO dye. On the other hand, hydrogen peroxide can be used as an electron remover, which can effectively inhibit the simple combination of photogenerated electrons (e^-) and photogenerated holes (h^+) on the surface of the catalyst, and improve the reaction rate of photocatalytic degradation. This may be due to the rapid formation of OH active groups on the surface of GO/TiO₂ by H₂O₂ to accelerate the degradation of MO.

Equations (1)–(7) and Fig. 5 show the pathway of electron transfer and mechanism of the degradation of MO dye by GO/TiO₂ composites. First, MO is adsorbed onto the surface of the GO/TiO₂ composites due to the π - π bond of graphene sheets. The GO/TiO₂ composites generate photogenerated electrons (e^-) and holes (h^+) on their surface under the irradiation of ultraviolet light. The water in the solution and the absorbed

OH⁻ on the surface of composites are the capture agent of photogenerated holes (h^+) to form the hydroxyl radical (\bullet OH). The free oxygen absorbed on the surface of nanocomposites react with photogenerated electrons (e^-) to obtain the H₂O₂, further forming \bullet OH. The \bullet OH is an active species and has a strong oxidation ability, and therefore can directly decompose the MO molecule. The GO promotes the contact between MO and TiO₂. In addition, GO, as the recipient of TiO₂ photogenerated electricity, effectively promotes the migration of photogenerated electrons and prevents the recombination of photogenerated electrons and holes. H₂O₂ as an electron remover effectively inhibits the simple combination of photogenerated electrons (e^-) and photogenerated holes (h^+) and promotes the increase in the number of hydroxyl radicals. So, the GO/TiO₂ nanocomposites exhibit excellent photocatalysis when adding H₂O₂, which can effectively decompose the MO dye.

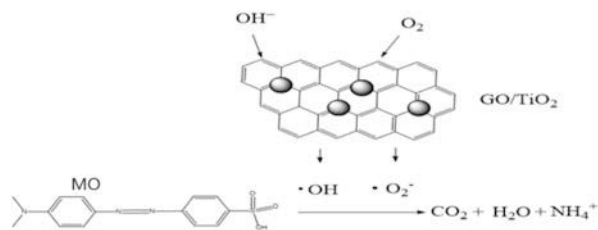
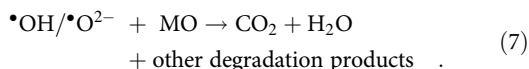
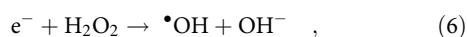
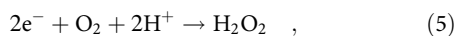
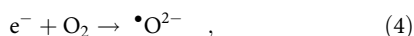
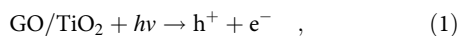


Figure 5: Pathways of electron transfer and mechanism of the degradation of MO dye.



Conclusion

In this article, GO/TiO₂ composites were prepared by the hydrothermal method, and the adsorption and degradation conditions of MO by GO/TiO₂ were studied. The specific surface area of GO/TiO₂ is about 152.5 m²/g, the pore volume is about 0.2199 cm³/g, and the pore size is 20–40 nm, which is a micro-mesoporous material. The adsorption and degradation rate of GO/TiO₂ was 85.62% under ultraviolet lamp irradiation for 4 h. Compared with the traditional photocatalyst TiO₂, the composite has a higher catalytic activity for MO under mild conditions. Experimental results demonstrated that the adsorption and degradation efficiency of GO/TiO₂ is higher than that of TiO₂. The H₂O₂ obviously improves the degradation efficiency of MO. The adsorption and degradation of GO/TiO₂ dioxide consists of two parts: the first pathway is the adsorption of MO molecules by GO/TiO₂ and the second is the chemical photodegradation of MO on GO surface.

Experimental section

Materials

MO was purchased from Sigma-Aldrich and was used without further purification. TiCl₃ (20–35%) was purchased from NANO Co. H₂O₂ (30%) was obtained from Duksan Pure

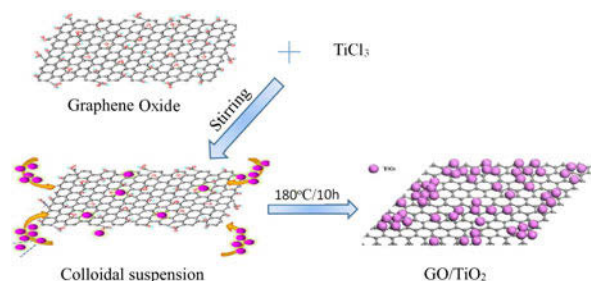


Figure 6: Synthetic scheme of GO/TiO₂ composites.

Chemical company. Graphite powder, KMnO₄, and H₂SO₄ were purchased from Kanto Chemical Co., Daejung Chemicals & Metals Co., and Yakuri Pure Chemicals Co., respectively.

Preparation of GO/TiO₂ nanocomposites

The synthesis of GO was conducted using the modified Hummers method with graphite powder as the raw materials according to the process described in the previous work [63, 64]. The synthesized GO was dispersed in 50 mL H₂O by ultrasonic treatment under ambient conditions to yield a brown GO dispersion. The GO/TiO₂ composites were fabricated by a hydrothermal reaction method. The concrete procedures were as follows. First, titanium tetrachloride (TiCl₃) solution (25–30%, 4 mL) was added into a three-neck flask, and then NH₃·H₂O solution (37%, 5 mL) was added dropwise into the TiCl₃ solution with vigorous agitation at ambient temperature to obtain a turbid solution. Subsequently, GO dispersion (100 mg/L, 100 mL) was added rapidly into the above solution to stir for 30 min. Then, the mixture was put into a hydrothermal reactor at 180 °C for 6 h. Finally, the product was filtrated and washed several times with deionized water and dried at 80 °C to obtain GO/TiO₂ composites. The preparation process for GO/TiO₂ nanocomposites was displayed in Fig. 6.

Characterization

The structure composition of samples was characterized by a Fourier transform-infrared (FTIR) spectrometer (FTS2000) with KBr pellets, scanning from 400 cm⁻¹ to 4000 cm⁻¹ at the resolution of 1.5 cm⁻¹ for eight times. The Raman spectra of GO and GO/TiO₂ composites were measured by using a RLX Renishaw 1000 Raman spectrometer with 514 nm of excitation wavelength. Thermalgravimetric analysis (TGA; Mettler Company, Jiangsu Science equipment Co., Ltd.) was conducted at a temperature range of 25–1000 °C and a heating rate of 15 °C/min. The crystalline phase of GO/TiO₂ composites was tested by X-ray diffractometer (XRD; XRD-600, Japan Shimadzu Co., Ltd.) scanning from 10° to 90° in the conditions of voltage of 40 kV, current of 30 mA, and scanning rate of 8°/min, respectively. The surface area and porosity measurements were

performed by N₂ adsorption at 0–300 °C range with an automated volumetric apparatus (ASAP2020, Micromeritics Instrument Ltd., USA). The surface morphology and microstructures of the GO/TiO₂ were investigated by using a scanning electron microscope (SEM; Apollo 300). The photocatalytic properties were tested by using an ultraviolet spectrophotometer UV-vis-L6S. The range of the wavelength test is 200–900 nm.

Photocatalytic degradation of MO

0.1 g sample was added into 100 mL of MO (20 mg/L) solution and the solution ultrasonic treated in the dark for 30 min. The solution was placed under sunlight or a 48W UV lamp with 240 nm wavelength with a 6-cm distance between the lamp tube and sample for different time periods. The solution was gathered every half hour and then centrifuged for 10 min to collect the supernatant used for measuring the absorbance by UV-vis spectrophotometry (721E Vis spectrophotometer) to detect the MO content. The degradation rate of MO was calculated by drawing a standard curve and formula.

$$D = (C_0 - C_1)/C_0 \times 100\% \quad ,$$

where D is the degradation ratio of MO, C_0 is the initial concentration of MO in the solution, and C_1 presents the equilibrium concentration of MO after photocatalytic degradation.

Acknowledgments

We gratefully acknowledge the support from the special fund of Shaanxi Provincial Education Department (16JK1612), the Key Laboratory of High-tech Research on Marine Functional Thin Film Materials in Zhenjiang (ZHZ2019008), the key research and development project of Shaanxi Province in 2017 (2017GY-180), and the Provincial College Students Innovation and Entrepreneurship Program (201819018).

References

1. S.D. Perera, R.G. Mariano, K. Vu, N. Nour, O. Seitz, Y. Chabal, and K.J. Balkus, Jr.: Hydrothermal synthesis of graphene–TiO₂ nanotube composites with enhanced photocatalytic activity. *ACS Catal.* **2**, 949 (2012).
2. F. Guo, W. Shi, X. Lin, and G. Che: Hydrothermal synthesis of graphitic carbon nitride–BiVO₄ composites with enhanced visible light photocatalytic activities and the mechanism study. *J. Phys. Chem. Solids* **75**, 1217 (2014).
3. Y. Huo, R. Hou, X. Chen, H. Yin, Y. Gao, and H. Li: BiOBr visible-light photocatalytic films in a rotating disk reactor for the degradation of organics. *J. Mater. Chem. A* **3**, 14801 (2015).
4. Q. Wang, S. Dong, D. Zhang, C. Yu, J. Lu, D. Wang, and J. Sun: Magnetically recyclable visible-light-responsive MoS₂@Fe₃O₄ photocatalysts targeting efficient wastewater treatment. *J. Mater. Sci.* **53**, 1135 (2018).
5. Z. Zhang, J. Zhang, S. Li, J. Liu, M. Dong, Y. Li, N. Lu, S. Lei, J. Tang, and J. Fan: Effect of graphene liquid crystal on dielectric properties of polydimethylsiloxane nanocomposites. *Composites, Part B* **176**, 107338 (2019).
6. L. Wang, H. Hu, J. Xu, S. Zhu, A. Ding, and C. Deng: WO₃ nanocubes: Hydrothermal synthesis, growth mechanism, and photocatalytic performance. *J. Mater. Res.* **34**, 2955 (2019).
7. W. Wang, J. Fang, S. Shao, M. Lai, and C. Lu: Compact and uniform TiO₂@g-C₃N₄ core-shell quantum heterojunction for photocatalytic degradation of tetracycline antibiotics. *Appl. Catal., B* **217**, 57 (2017).
8. H. Tong, S. Ouyang, Y. Bi, N. Umezawa, M. Oshikiri, and J. Ye: Nano-photocatalytic materials: Possibilities and challenges. *Adv. Mater.* **24**, 229 (2012).
9. S. Liu, Y. Wang, L. Ma, and H. Zhang: Ni₂P/ZnS(CdS) core/shell composites with their photocatalytic performance. *J. Mater. Res.* **33**, 3580 (2018).
10. H. Wang, K. Zhu, L. Yan, C. Wei, Y. Zhang, C. Gong, J. Guo, J. Zhang, D. Zhang, and J. Zhang: Efficient and scalable high-quality graphene nanodot fabrication through confined lattice plane electrochemical exfoliation. *Chem. Commun.* **55**, 5805 (2019).
11. Y. Wei, Y. Shi, Z. Jiang, X. Zhang, H. Chen, Y. Zhang, J. Zhang, and C. Gong: High performance and lightweight electromagnetic wave absorbers based on TiN/RGO flakes. *J. Alloys Compd.* **810**, 151950 (2019).
12. Y. Guo, K. Ruan, X. Yang, T. Ma, J. Kong, N. Wu, J. Zhang, J. Gu, and Z. Guo: Constructing fully carbon-based fillers with hierarchical structure to fabricate highly thermally conductive polyimide nanocomposites. *J. Mater. Chem. C* **7**, 7035 (2019).
13. W. Zhang, C. Wang, X. Liu, and J. Li: Enhanced photocatalytic activity in porphyrin-sensitized TiO₂ nanorods. *J. Mater. Res.* **32**, 2773 (2017).
14. X. Lang, X. Chen, and J. Zhao: Heterogeneous visible light photocatalysis for selective organic transformations. *Chem. Soc. Rev.* **43**, 473 (2014).
15. J. Schneider, M. Matsuoka, M. Takeuchi, J. Zhang, Y. Horiuchi, M. Anpo, and D.W. Bahnemann: Understanding TiO₂ photocatalysis: Mechanisms and materials. *Chem. Rev.* **114**, 9919 (2014).
16. J. Zhang, J. Yi, and Y. Jiao: Preparation and application of water-soluble TiO₂-ionic liquids hybrid nanomaterials. *J. Inorg. Mater.* **33**, 577 (2018).
17. Y. Guo, X. Yang, K. Ruan, J. Kong, M. Dong, J. Zhang, J. Gu, and Z. Guo: Reduced graphene oxide heterostructured silver nanoparticles significantly enhanced thermal conductivities in hot-pressed electrospun polyimide nanocomposites. *ACS Appl. Mater. Interfaces* **11**, 25465 (2019).
18. C. Liang, P. Song, A. Ma, X. Shi, H. Gu, L. Wang, H. Qiu, J. Kong, and J. Gu: Highly oriented three-dimensional structures

- of Fe₃O₄ decorated CNTs/reduced graphene oxide foam/epoxy nanocomposites against electromagnetic pollution. *Compos. Sci. Technol.* **181**, 107683 (2019).
19. C. Liang, P. Song, H. Qiu, Y. Zhang, X. Ma, F. Qi, H. Gu, J. Kong, D. Cao, and J. Gu: Constructing interconnected spherical hollow conductive networks in silver platelets/reduced graphene oxide foam/epoxy nanocomposites for superior electromagnetic interference shielding effectiveness. *Nanoscale* **11**, 22590 (2019).
 20. J. Zhang, W. Zhang, L. Wei, L. Pu, J. Liu, H. Liu, Y. Li, J. Fan, T. Ding, and Z. Guo: Alternating multilayer structural epoxy composite coating for corrosion protection of steel. *Macromol. Mater. Eng.* **304**, 1900374 (2019).
 21. Z. Lyu, B. Liu, R. Wang, and L. Tian: Synergy of palladium species and hydrogenation for enhanced photocatalytic activity of {001} facets dominant TiO₂ nanosheets. *J. Mater. Res.* **32**, 2781 (2017).
 22. L. Thirugnanam, S. Kaveri, M. Dutta, N.V. Jaya, and N. Fukata: Porous tubular rutile TiO₂ nanofibers: Synthesis, characterization and photocatalytic properties. *J. Nanosci. Nanotechnol.* **14**, 3034 (2014).
 23. S. Banerjee, S.C. Pillai, P. Falaras, K.E. O'shea, J.A. Byrne, and D.D. Dionysiou: New insights into the mechanism of visible light photocatalysis. *J. Phys. Chem. Lett.* **5**, 2543 (2014).
 24. M. Pelaez, N.T. Nolan, S.C. Pillai, M.K. Seery, P. Falaras, A.G. Kontos, P.S. Dunlop, J.W. Hamilton, J.A. Byrne, and K. O'shea: A review on the visible light active titanium dioxide photocatalysts for environmental applications. *Appl. Catal. B* **125**, 331 (2012).
 25. X. Wang, M. Utsumi, Y. Yang, D. Li, Y. Zhao, Z. Zhang, C. Feng, N. Sugiura, and J.J. Cheng: Degradation of microcystin-LR by highly efficient AgBr/Ag₃PO₄/TiO₂ heterojunction photocatalyst under simulated solar light irradiation. *J. Phys. Chem. Lett.* **325**, 1 (2015).
 26. P. Song, C. Liang, L. Wang, H. Qiu, H. Gu, J. Kong, and J. Gu: Obviously improved electromagnetic interference shielding performances for epoxy composites via constructing honeycomb structural reduced graphene oxide. *Compos. Sci. Technol.* **181**, 107698 (2019).
 27. X. Yang, S. Fan, Y. Li, Y. Guo, Y. Li, K. Ruan, S. Zhang, J. Zhang, J. Kong, and J. Gu: Synchronously improved electromagnetic interference shielding and thermal conductivity for epoxy nanocomposites by constructing 3D copper nanowires/thermally annealed graphene aerogel framework. *Composites, Part A* **128**, 105670 (2020).
 28. G. Liu, Y. Zhao, C. Sun, F. Li, G.Q. Lu, and H.M. Cheng: Synergistic effects of B/N doping on the visible-light photocatalytic activity of mesoporous TiO₂. *Angew. Chem., Int. Ed.* **47**, 4516 (2008).
 29. D.H. Kim, H.S. Hong, S.J. Kim, J.S. Song, and K.S. Lee: Photocatalytic behaviors and structural characterization of nanocrystalline Fe-doped TiO₂ synthesized by mechanical alloying. *J. Alloys Compd.* **375**, 259 (2004).
 30. L. Zhang, X. Li, Z. Chang, and D. Li: Preparation, characterization and photoactivity of hollow N, Co co-doped TiO₂/SiO₂ microspheres. *Mater. Sci. Semicond. Process.* **14**, 52 (2011).
 31. L.G. Devi and R. Kavitha: A review on non metal ion doped titania for the photocatalytic degradation of organic pollutants under UV/solar light: Role of photogenerated charge carrier dynamics in enhancing the activity. *Appl. Catal., B* **140**, 559 (2013).
 32. F. Huang, D. Chen, X.L. Zhang, R.A. Caruso, and Y.B. Cheng: Dual-function scattering layer of submicrometer-sized mesoporous TiO₂ beads for high-efficiency dye-sensitized solar cells. *Adv. Funct. Mater.* **20**, 1301 (2010).
 33. S. Wooh, T. Kim, D. Song, Y. Lee, T.K. Lee, V.W. Bergmann, S.A. Weber, J. Bisquert, Y.S. Kang, and K. Char: Surface modification of TiO₂ photoanodes with fluorinated self-assembled monolayers for highly efficient dye-sensitized solar cells. *ACS Appl. Mater. Interfaces* **7**, 25741 (2015).
 34. J. Zhang, S. Liu, C. Yan, X. Wang, L. Wang, Y. Yu, and S. Li: Abrasion properties of self-suspended hairy titanium dioxide nanomaterials. *Appl. Nanosci.* **7**, 691 (2017).
 35. Y. Xie, G. Ali, S.H. Yoo, and S.O. Cho: Sonication-assisted synthesis of CdS quantum-dot-sensitized TiO₂ nanotube arrays with enhanced photoelectrochemical and photocatalytic activity. *ACS Appl. Mater. Interfaces* **2**, 2910 (2010).
 36. A.A. Ismail, I. Abdelfattah, A. Helal, S. Al-Sayari, L. Robben, and D. Bahnemann: Easy synthesis of mesoporous WO₃-TiO₂ nanocomposites with enhanced photocatalytic performance for photodegradation of herbicide imazapyr under visible light and UV illumination. *J. Hazard. Mater.* **307**, 43 (2016).
 37. J. Sheng, H. Tong, H. Xu, and C. Tang: Preparation and photocatalytic activity of SnO₂@TiO₂ core-shell composites modified by Ag. *Catal. Surv. Asia* **20**, 167 (2016).
 38. J. Zhang, Z. Zhang, Y. Jiao, H. Yang, Y. Li, J. Zhang, and P. Gao: The graphene/lanthanum oxide nanocomposites as electrode materials of supercapacitors. *J. Power Sources* **419**, 99 (2019).
 39. Y. Jiao, J. Zhang, S. Liu, Y. Liang, S. Li, H. Zhou, and J. Zhang: The graphene oxide ionic solvent-free nanofluids and their battery performances. *Sci. Adv. Mater.* **10**, 1706 (2018).
 40. J. Paredes, S. Villar-Rodil, A. Martínez-Alonso, and J. Tascon: Graphene oxide dispersions in organic solvents. *Langmuir* **24**, 10560 (2008).
 41. J. Zhang, P. Li, Z. Zhang, X. Wang, J. Tang, H. Liu, Q. Shao, T. Ding, A. Umar, and Z. Guo: Solvent-free graphene liquids: Promising candidates for lubricants without the base oil. *J. Colloid Interface Sci.* **542**, 159 (2019).
 42. Y. Guo, G. Xu, X. Yang, K. Ruan, T. Ma, Q. Zhang, J. Gu, Y. Wu, H. Liu, and Z. Guo: Significantly enhanced and precisely modeled thermal conductivity in polyimide nanocomposites with chemically modified graphene via in situ polymerization and electrospinning-hot press technology. *J. Mater. Chem. C* **6**, 3004 (2018).
 43. Y. Li, T. Jing, G. Xu, J. Tian, M. Dong, Q. Shao, B. Wang, Z. Wang, Y. Zheng, and C. Yang: 3-D magnetic graphene oxide-

- magnetite poly(vinyl alcohol) nanocomposite substrates for immobilizing enzyme. *Polymer* **149**, 13 (2018).
44. **K. Sun, J. Dong, Z. Wang, Z. Wang, G. Fan, Q. Hou, L. An, M. Dong, R. Fan, and Z. Guo:** Tunable negative permittivity in flexible graphene/PDMS metamaterials. *J. Phys. Chem. C* **123**, 23635 (2019).
 45. **M. Idrees, S. Batool, J. Kong, Q. Zhuang, H. Liu, Q. Shao, N. Lu, Y. Feng, E.K. Wujcik, and Q. Gao:** Polyborosilazane derived ceramics-nitrogen sulfur dual doped graphene nanocomposite anode for enhanced lithium ion batteries. *Electrochim. Acta* **296**, 925 (2019).
 46. **V. Murugadoss, J. Lin, H. Liu, X. Mai, T. Ding, Z. Guo, and S. Angaiah:** Optimizing graphene content in a NiSe/graphene nanohybrid counter electrode to enhance the photovoltaic performance of dye-sensitized solar cells. *Nanoscale* **11**, 17579 (2019).
 47. **Y. He, Q. Chen, H. Liu, L. Zhang, D. Wu, C. Lu, W. OuYang, D. Jiang, M. Wu, and J. Zhang:** Friction and wear of MoO₃/graphene oxide modified glass fiber reinforced epoxy nanocomposites. *Macromol. Mater. Eng.* **304**, 1900166 (2019).
 48. **L. Ma, Y. Zhu, P. Feng, G. Song, Y. Huang, H. Liu, J. Zhang, J. Fan, H. Hou, and Z. Guo:** Reinforcing carbon fiber epoxy composites with triazine derivatives functionalized graphene oxide modified sizing agent. *Composites, Part B* **176**, 107078 (2019).
 49. **B. Kumar, D.K. Verma, A.K. Singh, Kavita, N. Shukla, and R.B. Rastogi:** Nanohybrid Cu@C: Synthesis, characterization and application in enhancement of lubricity. *Compos. Interfaces*, 1 (2019) doi.org/10.1080/09276440.2019.1697134.
 50. **C. Lou, T. Jing, J. Tian, Y. Zheng, J. Zhang, M. Dong, C. Wang, C. Hou, J. Fan, and Z. Guo:** 3-Dimensional graphene/Cu/Fe₃O₄ composites: Immobilized laccase electrodes for detecting bisphenol A. *J. Mater. Res.* **34**, 2964 (2019).
 51. **Y. He, Q. Chen, S. Yang, C. Lu, M. Feng, Y. Jiang, G. Cao, J. Zhang, and C. Liu:** Micro-crack behavior of carbon fiber reinforced Fe₃O₄/graphene oxide modified epoxy composites for cryogenic application. *Composites, Part A* **108**, 12 (2018).
 52. **M. Liu, Q. Meng, Z. Yang, X. Zhao, and T. Liu:** Ultra-long-term cycling stability of an integrated carbon-sulfur membrane with dual shuttle-inhibiting layers of graphene “nets” and a porous carbon skin. *Chem. Commun.* **54**, 5090 (2018).
 53. **B.S. Gonçalves, L.M. Silva, T.C. de Souza, V.G. de Castro, G.G. Silva, B.C. Silva, K. Krambrock, R.B. Soares, V.F. Lins, and M. Houmard:** Solvent effect on the structure and photocatalytic behavior of TiO₂-RGO nanocomposites. *J. Mater. Res.* **34**, 3918 (2019).
 54. **X. Yan, X. Yuan, J. Wang, Q. Wang, C. Zhou, D. Wang, H. Tang, J. Pan, and X. Cheng:** Construction of novel ternary dual Z-scheme Ag₃VO₄/C₃N₄/reduced TiO₂ composite with excellent visible-light photodegradation activity. *J. Mater. Res.* **34**, 2024 (2019).
 55. **V. Labunov, L. Tabulina, I. Komissarov, D. Grapov, E. Prudnikova, Y.P. Shaman, S. Basaev, and A. Pavlov:** Features of the reduction of graphene from graphene oxide. *Russ. J. Phys. Chem. A* **91**, 1088 (2017).
 56. **B. Cao, H. Liu, L. Yang, X. Li, H. Liu, P. Dong, X. Mai, C. Hou, N. Wang, and J. Zhang:** Interfacial engineering for high-efficiency nanorod array-structured perovskite solar cells. *ACS Appl. Mater. Interfaces*. **11**, 33770 (2019).
 57. **L. Yang, X. Wang, X. Mai, T. Wang, C. Wang, X. Li, V. Murugadoss, Q. Shao, S. Angaiah, and Z. Guo:** Constructing efficient mixed-ion perovskite solar cells based on TiO₂ nanorod array. *J. Colloid Interface Sci.* **534**, 459 (2019).
 58. **L. Zhang, M. Qin, W. Yu, Q. Zhang, H. Xie, Z. Sun, Q. Shao, X. Guo, L. Hao, and Y. Zheng:** Heterostructured TiO₂/WO₃ nanocomposites for photocatalytic degradation of toluene under visible light. *J. Electrochem. Soc.* **164**, H1086 (2017).
 59. **L. Zhang, W. Yu, C. Han, J. Guo, Q. Zhang, H. Xie, Q. Shao, Z. Sun, and Z. Guo:** Large scaled synthesis of heterostructured electrospun TiO₂/SnO₂ nanofibers with an enhanced photocatalytic activity. *J. Electrochem. Soc.* **164**, H651 (2017).
 60. **L. Shindume, Z. Zhao, N. Wang, H. Liu, A. Umar, J. Zhang, T. Wu, and Z. Guo:** Enhanced photocatalytic activity of B, N-codoped TiO₂ by a new molten nitrate process. *J. Nanosci. Nanotechnol.* **19**, 839 (2019).
 61. **J. Tian, Q. Shao, J. Zhao, D. Pan, M. Dong, C. Jia, T. Ding, T. Wu, and Z. Guo:** Microwave solvothermal carboxymethyl chitosan templated synthesis of TiO₂/ZrO₂ composites toward enhanced photocatalytic degradation of rhodamine B. *J. Colloid Interface Sci.* **541**, 18 (2019).
 62. **L. Ma, N. Li, G. Wu, G. Song, X. Li, P. Han, G. Wang, and Y. Huang:** Interfacial enhancement of carbon fiber composites by growing TiO₂ nanowires onto amine-based functionalized carbon fiber surface in supercritical water. *Appl. Surf. Sci.* **433**, 560 (2018).
 63. **S. Stankovich, D.A. Dikin, R.D. Piner, K.A. Kohlhaas, A. Kleinhammes, Y. Jia, Y. Wu, S.T. Nguyen, and R.S. Ruoff:** Synthesis of graphene-based nanosheets via chemical reduction of exfoliated graphite oxide. *Carbon* **45**, 1558 (2007).
 64. **J. Zhang, Y. Liang, X. Wang, H. Zhou, S. Li, J. Zhang, Y. Feng, N. Lu, Q. Wang, and Z. Guo:** Strengthened epoxy resin with hyperbranched polyamine-ester anchored graphene oxide via novel phase transfer approach. *Adv. Compos. Hybrid Mater.* **1**, 300 (2018).